Journal of Alloys and Compounds 509 (2011) 8382–8386

Contents lists available at ScienceDirect

Journal of Alloys and Compounds

journal homepage: www.elsevier.com/locate/jallcom

Cobalt–iron cyanide hollow cubes: Three-dimensional self-assembly and magnetic properties

Chuanxin Zhai, Ning Du*, Hui Zhang, Deren Yang

State Key Lab of Silicon Materials and Department of Materials Science and Engineering, Zhejiang University, Hangzhou 310027, People's Republic of China

ARTICLE INFO

Article history:
Received 24 February 2011
Received in revised form 17 May 2011
Accepted 18 May 2011
Available online 27 May 2011

Keywords:
Hollow cubes
Self-assembly
Solvothermal
Magnetic properties

ABSTRACT

Cobalt–iron cyanide hollow cubes have been synthesized via a poly(vinylpyrrolidone) assisted solvothermal route. A unique formation process: self-assembly followed by Ostwald ripening process, has been put forward to take account for the construction of hollow cubes. The rod-like nanocrystals first assemble as porous cubes via an oriented attachment process. Then, the porous cubes undergo an Ostwald-ripening process, which create interior spaces and result in the formation of hollow cubes. The magnetic property investigation reveals that $K_{0.22}Co_{0.58}Fe_{2.2}(CN)_6$ hollow cubes exhibit a ferromagnetic behavior.

1. Introduction

Since novel properties of nanomaterials depend on morphology, many attentions have been paid on the fabrication of nanomaterials with different sizes and shapes [1–5]. Among a large variety of nanomaterials with distinct geometric shapes, the ones which have hollow interiors such as nanotubes, hollow cubes and hollow spheres are becoming more and more attractive [6–24]. Owing to their unique structures and properties, hollow nanostructures have been considered to have the potential applications in different technological fields, such as drug delivery [13], sensors [8,16] and energy storage [11,17,23]. Therefore, designing, controlling and understanding the growth process of hollow nanostructures have been recognized as a significant subject.

Up to now, two synthetic strategies can be employed to create nanostructures with hollow interiors. First, the template-assisted method was widely used to synthesize nanotubes, hollow nanospheres and other hollow structures by utilizing either hard templates such as carbon nanotubes and anodized aluminum oxide or soft templates such as surfactant micelles and bubbles [6,7,11,16,17,22]. Second, template-free synthesis was also employed to create interior spaces, which includes various physicochemical processes such as Ostwald ripening [9,23–25], Kirkendall effect [14,18], and oriented attachment [10,12] alongside with redox reaction.

Prussian blue and its analogues ($C_mM_x[M'(CN)_6]_y \cdot nH_2O$, C = Na^+, K^+, Cs^+; M = Mn, Co, Ni, Cu, Zn, Cd; M′ = Fe, Co) are probably the earliest synthetic coordination compounds. In recent years, cyanometalate-based coordination compounds have attracted much interest due to their fascinating magnetic properties [26–32]. The Prussian blue family exhibits not only spontaneous magnetization below T_C but also responds to external stimuli such as light, humidity, and pressure which make it possible to have potential applications in catalysis, sensors, batteries and photochemistry [33–36]. Photo-induced magnetization has been observed in one kind of the cobalt–iron Prussian blue analogues [27]. These photo-controllable magnetic materials are important in the development of photonic devices, such as erasable optical memory media and optical switching components. Moreover, tailoring the morphologies of Prussian blue analogue nanostructures is also a fascinating field in nanomaterial researches [37–40].

Herein, we present a novel approach to synthesize cobalt–iron Prussian blue hollow cubes. As depicted in Fig. 1, the formation of the hollow cubes is a unique process combined of both oriented attachment and Ostwald ripening processes. First, the rod-like nanocrystals assemble as porous cubes via an oriented attachment process. In the second stage, the porous cubes undergo an Ostwald-ripening process, which create interior spaces and result in the formation of hollow cubes. At last, the magnetic properties of the as-synthesized cobalt–iron cyanide hollow cubes were investigated.

* Corresponding author. Tel.: +86 571 87953190; fax: +86 571 87952322.
E-mail address: dna1122@zju.edu.cn (N. Du).

0925-8388/$ – see front matter © 2011 Elsevier B.V. All rights reserved.
doi:10.1016/j.jallcom.2011.05.073

2. Experimental

2.1. Materials synthesis

All the reagents used in the experiments were analytical grade and used without any further purification. The synthetic details were as follows: first, 0.474 g $CoCl_2 \cdot 6H_2O$ and 0.2 g polyvinyl pyrrolidone (PVP) was dissolved in the organic solvent N,N-dimethylformamide (DMF) to make a stated concentration. Then, 10 ml 0.2 M aqueous $K_3Fe(CN)_6$ solution was introduced to form a homogeneous suspension. Finally, 10 ml 85% $N_2H_4 \cdot H_2O$ was dropwise added into the above-mentioned suspension under vigorous stirring, which was then transferred into Teflon-lined stainless steel autoclaves, sealed and maintained at 200 °C for 20 h. After the reaction was complete, the resultant solid products were centrifugalized, washed with distilled water and ethanol to remove the ions possibly remaining in the final products, and dried at 60 °C in air.

2.2. Materials characterization

The products were characterized by X-ray powder diffraction (XRD) using a Rigaku D/max-ga X-ray diffractometer with graphite monochromatized Cu Kα radiation (λ = 1.541 78 Å). The images of the samples were obtained by a field emission scanning electron microscope (FESEM, FEI SIRION), a transmission electron microscope (TEM, JEM 200 CX 160 kV) and a high resolution transmission electron microscope (HRTEM, JEOL JEM-2010F). The magnetic properties were measured by Superconducting Quantum Interference Device (SQUID) and Physical Property Measurement System (PPMS-9, Quantum Design).

3. Results and discussion

Fig. 2 shows results of the morphological and structural characterizations of the sample prepared by the above-mentioned PVP-assisted solvothermal process at 200 °C for 20 h. The XRD pattern (Fig. 2a) shows that the products share the same crystal structure of a cobalt ferrite Prussian blue analogue (space group: F−43m; 10.08 Å; JCPDS 75-0038), indicating the synthesis of pure-phase Prussian blue. As can be seen from typical SEM image of the final products (Fig. 2b), large amounts of cubes with sizes of 200–400 nm were observed. Some broken cubes can be found with the interior spaces, indicating the formation of hollow cubes. Fig. 2c shows the TEM image of an individual cube. It can be seen that the interior space exists in the cube, which is consistent with the SEM image. The crystal orientation and crystallinity of the hollow cubes were further studied by HRTEM/SAED analysis (Fig. 2d). The clear diffraction spots indicate that the hollow cubes are single-crystalline. Moreover, the lattice fringes with lattice spacings of 0.50 nm corresponds to the {2 0 0} planes, which is in good agreement with the lattice reported in the literature (JCPDS files of 75-0038).

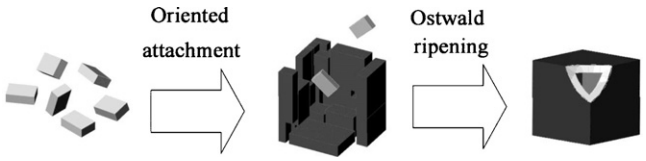

Fig. 1. Schematic illustration for the growth mechanism of the hollow cubes.

Fig. 3 shows the EDX spectrum of as-prepared cobalt–iron cyanide hollow cubes. It reveals the presence of K, Co, Fe, C, N, Al and Si (Al and Si are from the underlay of the sample in SEM).

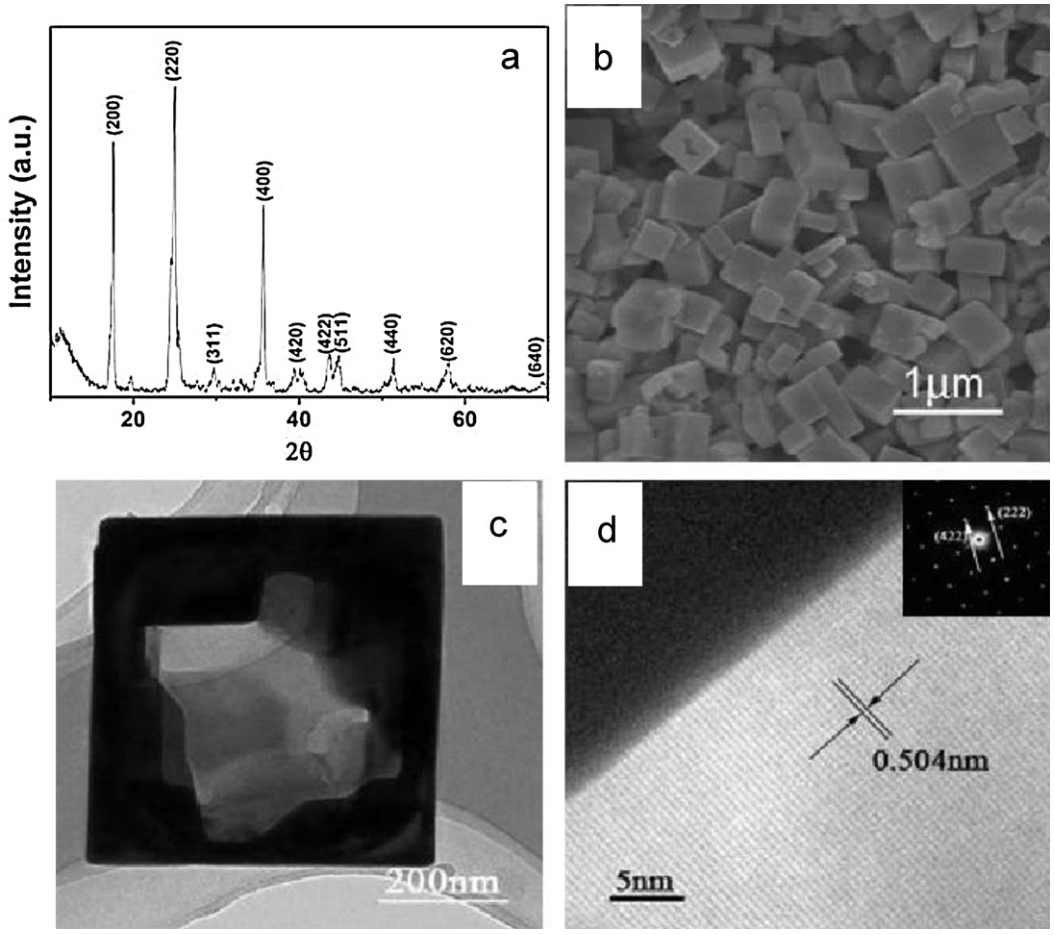

Fig. 2. Morphological and structural characterizations of the hollow cubes: (a) XRD pattern; (b) SEM image; (c) TEM image; (d) HRTEM image and SAED pattern.

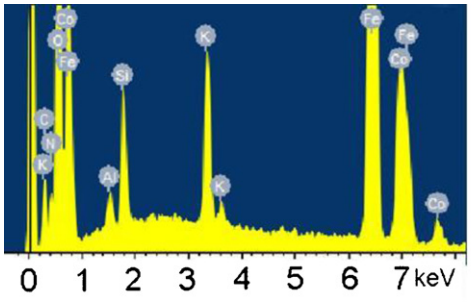

Element	Atomic Ratio (%)
C	29.9
N	23.2
K	3.5
Fe	34.6
Co	8.7

Fig. 3. EDX spectrum of as-prepared $K_{0.22}Co_{0.58}Fe_{2.2}(CN)_6$ hollow cubes.

The composition of the cobalt ferrite Prussian blue analogue can be confirmed as $K_{0.22}Co_{0.58}Fe_{2.2}(CN)_6$ from the atomic ratio in the EDX spectrum.

In order to clarify the formation process of the $K_{0.22}Co_{0.58}Fe_{2.2}(CN)_6$ hollow cubes during the solvothermal process, the products with different reaction times were taken out for TEM and SEM characterizations. After 2 h reaction, TEM and SEM images (Fig. 4a and b) show that rod-like $K_{0.22}Co_{0.58}Fe_{2.2}(CN)_6$ nanocrystallites were formed. The nanorods were about 50–100 nm in diameter and 200–300 nm in length. Fig. 4c and d shows the morphological characterizations of the products formed at the reaction time of 4 h. As can be seen, cube-like aggregates with the size of 200–400 nm were synthesized, which is self-assembled from the nanorods. The morphology of the rod-like precursors can be clearly identified in Fig. 4c. Moreover, there are a lot of intercrystallite spaces existing in these premature cubic structures. Three-dimension frames and

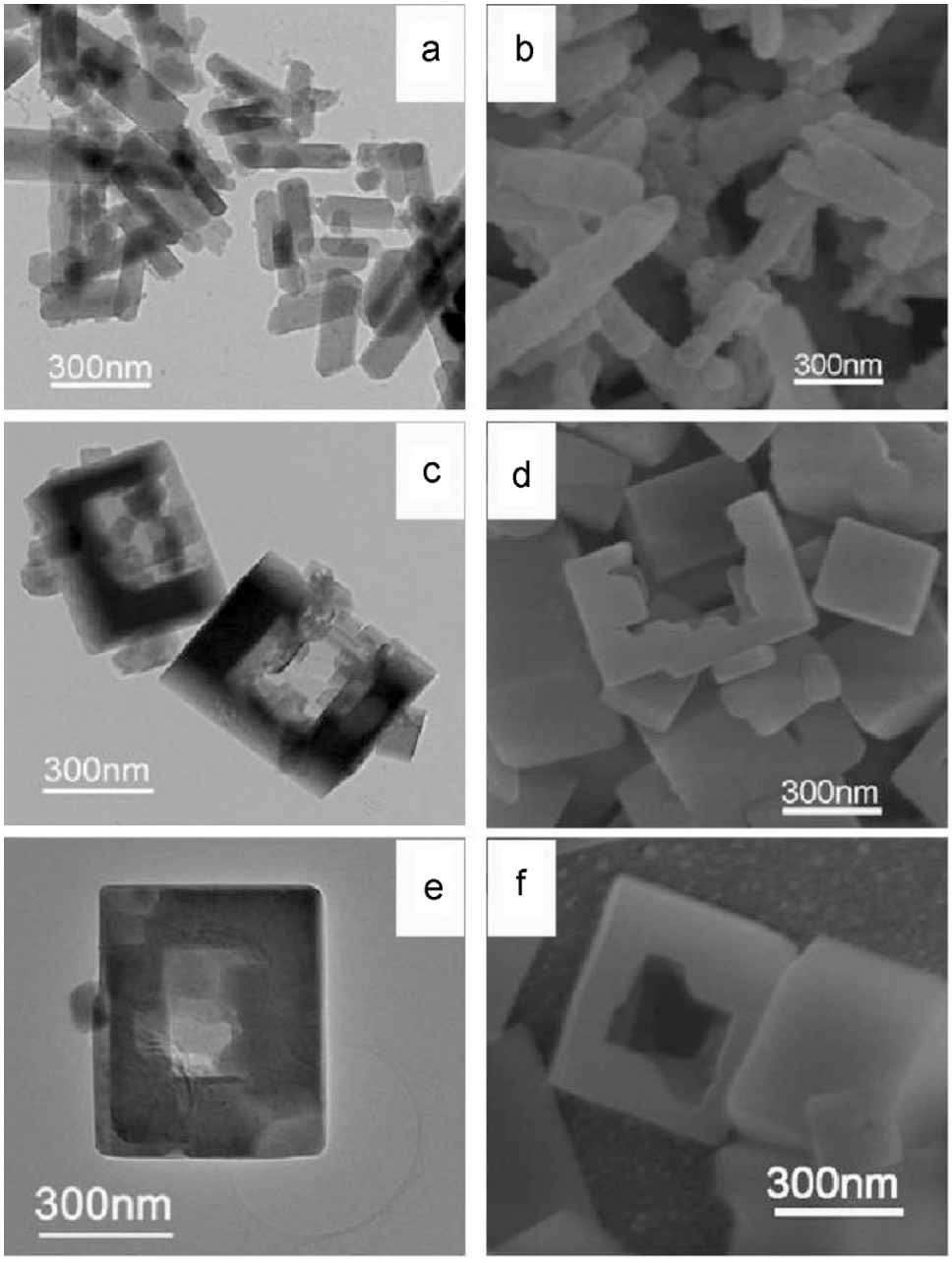

Fig. 4. TEM and SEM images of the products with different solvothermal reaction times: (a and b) 2 h; (c and d) 4 h; (e and f) 20 h.

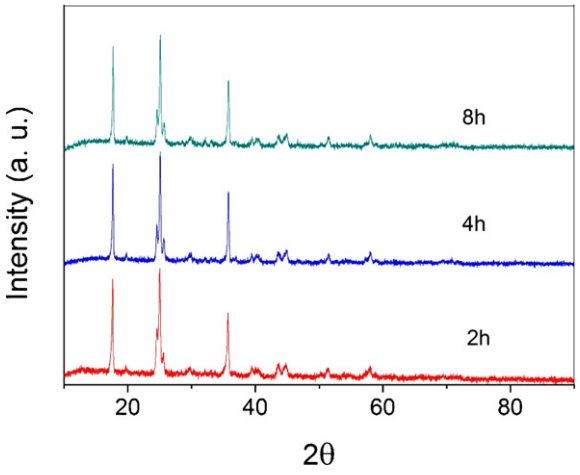

Fig. 5. XRD patterns of the products with different solvothermal reaction times.

porous cubes formed in sequence as the self-assemble process carrying on. During the next several hours' reaction, hollowing and recrystallization take place with Ostwald ripening, through which a central space is created and well crystallized single-crystalline cubes are formed as shown in Fig. 4e and f.

Corresponding to the morphology evolution, the XRD patterns of the products with different solvothermal reaction times are shown in Fig. 5. It can be seen that there are few differences between the XRD patterns. The phase of $K_{0.22}Co_{0.58}Fe_{2.2}(CN)_6$ formed within 2 h and remained no change in the next few hours. Based on the morphology and phase evolution as described above, the growth mechanism of the $K_{0.22}Co_{0.58}Fe_{2.2}(CN)_6$ hollow cubes can be summarized as the following three consecutive steps as illustrated in Fig. 1: (i) production of primary rod-like nanocrystallites; (ii) formation of polycrystalline cubic frames self-assembled from nanorods; and (iii) perfection of hollow cubes through an Ostwald process. A similar process combined of an oriented attachment and an Ostwald ripening has been also discovered as a possible way to provide hollow cubes and hollow spheres of Cu_2O [15,19].

Although the exact mechanism for the growth of $K_{0.22}Co_{0.58}Fe_{2.2}(CN)_6$ hollow cubes is not clear, it is found that the reactants such as PVP, N_2H_4, and DMF play the critical roles in the formation of $K_{0.22}Co_{0.58}Fe_{2.2}(CN)_6$ hollow cubes. PVP and DMF were usually employed to synthesize hollow nanostructures as reported previously [15,41]. PVP acted as the soft template to tune the morphology of nanostructures, while DMF acted not only as the solvent but also as the weak reducing agent. Herein, we believe that PVP and DMF play similar roles in the ripening process of the hollow structures. To further demonstrate this hypothesis, a comparison experiment has been carried out in absence of PVP and DMF. From the TEM and SEM images (Fig. 6), micrometre-sized cubes and random shaped polyhedrons were observed. However, no hollow structures were found without PVP and DMF. In addition, the presence of N_2H_4 ensured the formation of $K_{0.22}Co_{0.58}Fe_{2.2}(CN)_6$ under the solvothermal condition due to its reducing and mineralizing abilities. Moreover, it is believed that the extremely low solubility of $K_{0.22}Co_{0.58}Fe_{2.2}(CN)_6$ blue prefers the oriented attachment process to the classic dissolve-recrystallize crystallization [42].

The magnetic measurements for the $K_{0.22}Co_{0.58}Fe_{2.2}(CN)_6$ hollow cubes were performed on SQUID. Fig. 7a shows the curves of magnetization versus applied magnetic field at 2 and 300 K. As can be seen, both the *M–H* curves at 2 and 300 K exhibit a typical hysteresis loop with remanent magnetization and coercivity values, indicating the ferromagnetic behavior of the $K_{0.22}Co_{0.58}Fe_{2.2}(CN)_6$ hollow cubes in this temperature range. The temperature dependence of the magnetization of the sample in the temperature range of 2–300 K was further characterized by the zero-field cooling (ZFC) and field cooling (FC) procedures in an applied magnetic field of 200 Oe, as shown in Fig. 7b. It is found that the ZFC curve gradually deviates from the FC curve at the temperatures below 300 K. Therefore, the ZFC and FC analyses further confirm the ferromagnetic behavior of the $K_{0.22}Co_{0.58}Fe_{2.2}(CN)_6$ hollow cubes. Fig. 8 shows the *M–H* curves at 300 K of intermediate products with solvothermal reaction time of 2 and 4 h, respectively. As can be seen, both the *M–H* curves exhibit typical hysteresis loops similar as the hollow cubes, which indicate their ferromagnetic nature. It is worth noting that the saturation magnetization and coercivity increase with the morphology evolution. We believe that the perfection of the crystal quality and the decrease of the surface broken bonds lead to the increase of the saturation magnetization and coercivity [43].

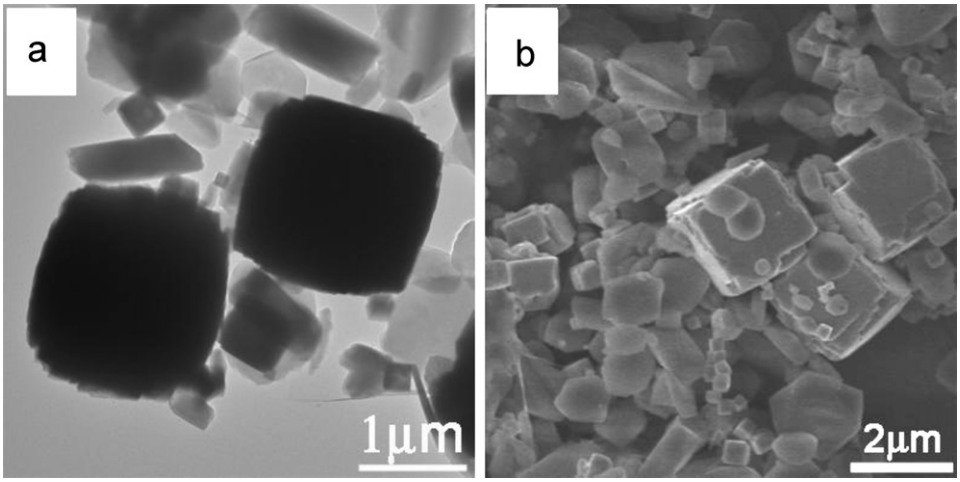

Fig. 6. (a) TEM and (b) SEM images of the products prepared in the absence of PVP and DMF.

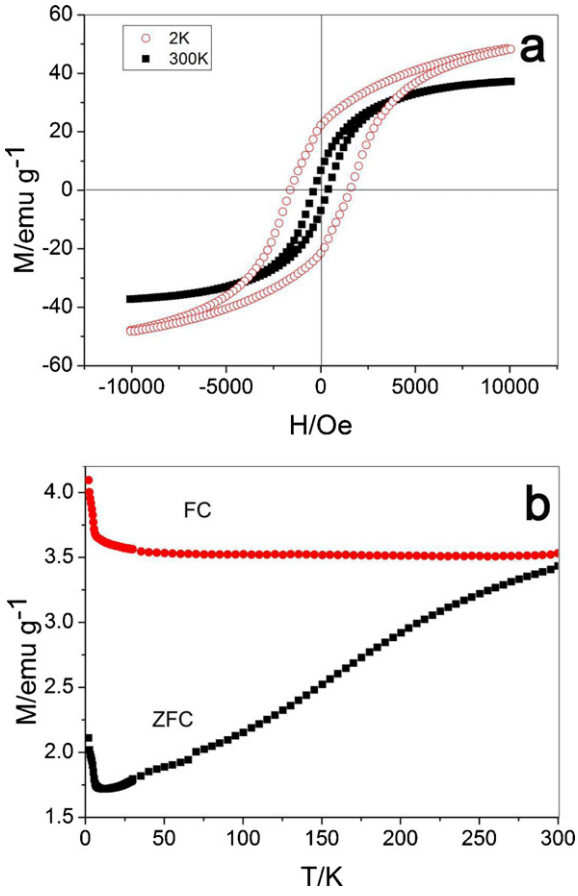

Fig. 7. The *M–H* curves at 2 and 300 K (a) and ZFC–FC curves with applied field of 200 Oe (b) of the $K_{0.22}Co_{0.58}Fe_{2.2}(CN)_6$ hollow cubes.

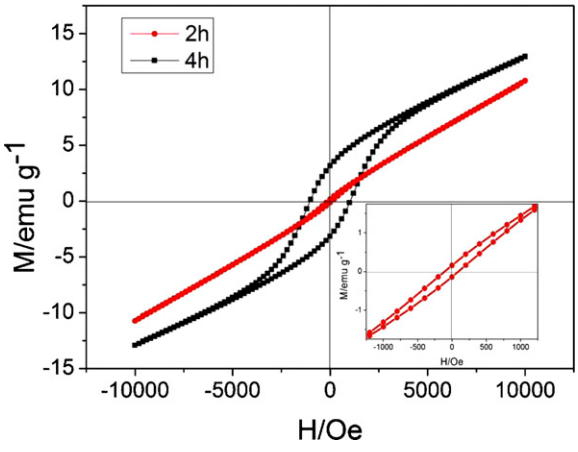

Fig. 8. The *M–H* curves at 300 K of products with different solvothermal reaction time. The inserted graph is the expanded view for the 2 h sample.

4. Conclusions

The $K_{0.22}Co_{0.58}Fe_{2.2}(CN)_6$ hollow cubes have been synthesized through the PVP assisted solvothermal process using DMF as the solvent. A self-assembly process followed by an Ostwald ripening process has been put forward to take account for growth of hollow cubes. Moreover, the $K_{0.22}Co_{0.58}Fe_{2.2}(CN)_6$ hollow cubes exhibit the ferromagnetic behavior at both 2 K and 300 K, which could find potential applications in high-density magnetic storage media, and high-performance electromagnetic and spintronic devices.

Acknowledgments

The authors would like to appreciate the financial supports from 973 Project (No. 2007CB613403), 863 Project (No. 2007AA02Z476), NSFC (No. 50802086), and China Postdoctoral Science Foundation funded project (No. 20090461350).

References

[1] A.P. Alivisatos, Science 271 (1996) 933.
[2] X. Peng, L. Manna, W. Yang, J. Wickham, E. Scher, A. Kadavanich, A.P. Alivisatos, Science 404 (2000) 59.
[3] Y. Sun, Y. Xia, Science 298 (2002) 2176.
[4] C. Burda, X. Chen, R. Narayanan, M.A. El-Sayed, Chem. Rev. 105 (2005) 1025.
[5] X. Wang, J. Zhuang, Q. Peng, Y. Li, Nature 437 (2005) 121.
[6] B.C. Satishkumar, A. Govindaraj, E.M. Vogl, L. Basumallick, C.N.R. Rao, J. Mater. Res. 12 (1997) 604.
[7] J. Sha, J. Niu, X. Ma, J. Xu, X. Zhang, Q. Yang, D. Yang, Adv. Mater. 14 (2002) 1219.
[8] X. Li, T. Lou, X. Sun, Y. Li, Inorg. Chem. 17 (2004) 43.
[9] H. Yang, H. Zeng, J. Phys. Chem. B 108 (2004) 3492.
[10] H. Yang, H. Zeng, Angew. Chem. Int. Ed. 43 (2004) 5930.
[11] X. Li, F. Cheng, B. Guo, J. Chen, J. Phys. Chem. B 109 (2005) 14017.
[12] M. Mo, J.C. Yu, L. Zhang, S.-K.A. Li, Adv. Mater. 17 (2005) 756.
[13] S.J. Son, J. Reichel, B. He, M. Schuchman, S.B. Lee, J. Am. Chem. Soc. 127 (2005) 7316.
[14] H. Fan, M. Knez, R. Scholz, K. Nielsch, E. Pippel, D. Hesse, M. Zacharias, U. Gosele, Nat. Mater. 5 (2006) 627.
[15] J.J. Teo, Y. Chang, H.C. Zeng, Langmuir 22 (2006) 7369.
[16] N. Du, H. Zhang, B. Chen, X. Ma, Z. Liu, J. Wu, D. Yang, Adv. Mater. 19 (2007) 1641.
[17] N. Du, H. Zhang, B. Chen, J. Wu, X. Ma, Z. Liu, Y. Zhang, D. Yang, X. Huang, J. Tu, Adv. Mater. 19 (2007) 4505.
[18] N. Du, H. Zhang, B. Chen, X. Ma, D. Yang, Chem. Commun. (2008) 3028.
[19] H. Xu, W. Wang, L. Zhou, Cryst. Growth Des. 8 (2008) 3486.
[20] L. Chen, H. Dai, Y. Shen, J. Bai, J. Alloys Compd. 491 (2010) L33–L38.
[21] X. Feng, L. Yang, N. Zhang, Y. Liu, J. Alloys Compd. 506 (2010) 728–733.
[22] G. Jia, C. Zhang, L. Wang, S. Ding, H. You, J. Alloys Compd. 509 (2011) 6418–6422.
[23] X. Guan, L. Li, G. Li, Z. Fu, J. Zheng, T. Yan, J. Alloys Compd. 509 (2011) 3367–3374.
[24] W. Li, X. Qiao, Q. Zheng, T. Zhang, J. Alloys Compd. 509 (2011) 6206–6211.
[25] H. Zhang, C. Zhai, J. Wu, X. Ma, D. Yang, Chem. Commun. (2008) 5648.
[26] O. Sato, T. Iyoda, A. Fujishima, K. Hashimoto, Science 271 (1996) 49.
[27] O. Sato, T. Iyoda, A. Fujishima, K. Hashimoto, Science 272 (1996) 704.
[28] M. Taguchi, I. Yagi, M. Nakagawa, T. Iyoda, Y. Einaga, J. Am. Chem. Soc. 128 (2006) 10978.
[29] S.M. Holmes, G.S. Girolami, J. Am. Chem. Soc. 121 (1999) 5593.
[30] L.G. Beauvais, J.R. Long, Inorg. Chem. 45 (2006) 236.
[31] Y. He, G. Tang, F. Liang, Y. Huang, M. Huang, J. Alloys Compd. 438 (2007) 52–55.
[32] S. Mat'aš, V. Kavečanský, M. Lukáčová, M. Mihalik, Z. Mitróová, M. Zentková, J. Alloys Compd. 459 (2008) 526–530.
[33] W. Buschmann, J. Miller, Inorg. Chem. 38 (1999) 4405.
[34] S. Han, Y. Chen, R. Pang, P. Wan, M. Fan, Ind. Eng. Chem. Res. 46 (2007) 6847.
[35] M. Jayalakshmi, F. Scholz, J. Power Sources 87 (2000) 212.
[36] G. Rogez, A. Marvilliers, E. Rivière, J.-P. Audière, F. Lloret, F. Varret, A. Goujon, N.T. Mallah, Angew. Chem. Int. Ed. 39 (2000) 2885.
[37] X. Roy, L.K. Thompson, N. Coombs, M.J. MacLachlan, Angew. Chem. Int. Ed. 47 (2008) 511.
[38] A. Johansson, E. Widenkvist, J. Lu, M. Boman, U. Jansson, Nano Lett. 5 (2005) 1603.
[39] G. Liang, J. Xu, X. Wang, J. Am. Chem. Soc. 131 (2009) 5378.
[40] J. Zhang, W. Yang, H. Zhu, J. Li, F. Yang, B. Zhang, X. Yang, J. Colloid Interface Sci. 338 (2009) 319.
[41] A. Cao, J. Hu, H. Liang, L. Wan, Angew. Chem. Int. Ed. 44 (2005) 4391.
[42] X. Zheng, Q. Kuang, T. Xu, Z. Jiang, S. Zhang, Z. Xie, R. Huang, L. Zheng, J. Phys. Chem. C 111 (2007) 4499.
[43] H. Shim, P. Dutta, M. Seehra, J. Bonevich, Solid State Commun. 145 (2008) 192.